Electonic Supporting Information

Dynamics of Caged Imidazolium Cation – Toward Understanding The Order-Disorder Phase Transition and Switchable Dielectric Constant†

Xi Zhang,[a] Xiu-Dan Shao,[b] Si-Chao Li,[b] Ying Cai,[b] Ye-Feng Yao,*[a] Ren-Gen Xiong[b] and Wen Zhang*[b]

Contents:

Experimental Section.

Figure S1. Temperature dependence of cell parameters of **1-d$_0$**.

Figure S2. Temperature-dependent dielectric constants (ε′) of **1-d$_0$** along the [101] direction measured at different frequencies.

Figure S3. Temperature-dependent dielectric constants (ε′) of **1-d$_0$** along the [001] direction measured at different frequencies.

Figure S4. DSC curves of **1-d$_3$**.

Figure S5. Axial motion of imidazolium cation (Model I). The simulated ^{2}H patterns show the influence of the angle, θ, between the rotational axis (C_n) and the molecular plane of imidazolium cation on the ^{2}H NMR lineshape. The quadrupole coupling used in the simulation is 144 kHz and the asymmetric parameter $\eta = 0$. The rotational frequency used in the simulation is 3 MHz.

Figure S6. Motion mode of imidazolium cation in ITP (Model II). In this model, the imidazolium ring perform an axial rotation combined an out-plane oscillatory fluctuation. In the simulation, the axail rotation of imidazolium cation is assumed to be in the fast limit and the fluctuation angle is assumed to have a Gaussian distribution with a width of σ. Because N-C**D**-N and N-C**D**-C**D**-N of deuterated imidazolium (**1-d$_3$**) are likely to have different quandrupole couplings, the right simulated pattern (gray)

was obtained by summating two patterns that were simulated by using the quadrupole couplings of 138 kHz and 144 kHz, respectively, and $\sigma = 12°$ in both cases. In the summation, the ratio of the two sub-patterns is 1:2. The lineshape of the simulated pattern (gray) closely resembles to the experimental pattern (black) acquired at 220 K.

Figure S7. Left: the experimental ^2H patterns at the temperature range between 190 K and 340 K. **Right**: the simulated ^2H patterns based on Model II (i.e., the axial C_n rotation + the out-plane oscillatory fluctuation). Each simulated pattern consists of two sub-patterns simulated by using the quadrupole couplings of 138 kHz and 144 kHz, respectively, and by assuming the fluctation angle having a Gaussian distribution with a width of σ. In the simulation, the axail C_n rotation is assumed to be in the fast limit. In the summation, the ratio of the two sub-patterns is 1:2.

Figure S8. Solid state ^2H magic angle spinning spectrum of **1-d_3**. The spectrum was measured using single pulse excitation. In the experiment, the rotation speed is 2.5 kHz and the recycle delay is 5 s. The experimental temperature is 280 K.

Figure S9. The centres of the equivalent negative charge and the positive charge of the HIm ring of the cage in HTP are shown as red balls with a distance of 0.036 Å.

Experimental Section

All reagents and solvents in the syntheses were of reagent grade and used without further purification. Evaporation of the aqueous solution (80 mL) of $K_3[Co(CN)_6]$ (3.32 g, 10 mmol) and (HIm)Cl (3.13 g, 30 mmol) results in the formation of **1** as pale-yellow crystals. Yield: 75 % (based on $K_3[Co(CN)_6]$). IR (cm^{-1}): 3402, 2155, 2120, 1608, 1439, 1023, 773.

Measurement Methods. Infrared spectroscopy studies were performed on a Shimadzu IRPrestige-21 spectrometer in the 4000–400 cm^{-1} region. Differential scanning calorimetry (DSC) measurement was performed on a PerkinElmer Diamond DSC under nitrogen atmosphere in aluminum crucibles with a heating or cooling rate of 10 K min^{-1}. Specific heat (C_p) measurement was carried out on a Quantum Design PPMS. For dielectric measurements the samples were made with the single crystal sample of **1-d$_0$** along the pre-determined axis. Silver conduction paste deposited on the surfaces was used as the electrodes. Complex dielectric permittivities were measured with an Agilent 4294A impedance analyzer over the frequency range of from 0.1 kHz to 1 MHz with an applied electric field of 0.5 V.

Single-Crystal X-ray Crystallography. X-ray diffraction experiments were carried out on **1-d$_0$** using a Rigaku Saturn 924 diffractometer with Mo-Kα radiation (λ = 0.71073 Å) at various temperatures. Data collection, cell refinement and data reduction were performed by using CrystalClear software package (Rigaku). The structures of **1-d$_0$** were solved by direct methods and refined by the full-matrix method based on F^2 using the SHELXLTL software package. All non-hydrogen atoms were refined anisotropically and the positions of all hydrogen atoms were generated geometrically. Crystal data for **1-d$_0$** at 293 K: $C_{10}H_{10}CoKN_{10}$, M_w = 392.33, trigonal $R\bar{3}m$, $a = b$ = 8.715(1) Å, c = 19.011(4) Å, V = 1250.5(3) $Å^3$, Z = 3, D_c = 1.563 Mg m^{-3}, R_1 ($I > 2\sigma$) = 0.0302, wR_2 = 0.0969, μ = 1.296 mm^{-1}, S = 1.327; **1-d$_0$** at 148 K: trigonal $R\bar{3}m$, $a = b$ = 8.738(6) Å, c = 18.71(1) Å, V = 1237(1) $Å^3$, Z = 3, D_c = 1.580 Mg m^{-3}, R_1 ($I > 2\sigma$) = 0.0589, wR_2 = 0.1399, μ = 1.310 mm^{-1}, S = 1.255; **1-d$_0$** at 93 K: monoclinic $C2/c$, a =

13.427(3) Å, b = 8.732(2) Å, c = 15.083(3) Å, β = 111.70(3)º, V = 1643.1(6) Å^3, Z = 4, D_c = 1.568 Mg m^{-3}, R_1 ($I > 2\sigma$) = 0.0614, wR_2 = 0.1311, μ = 1.315 mm^{-1}, S = 1.113.

CCDC 1012553−1012555 contains the supplementary crystallographic data for this paper. These data can be obtained free of charge from The Cambridge Crystallographic Data Centre via www.ccdc.cam.ac.uk/data_request/cif (or from the Cambridge Crystallographic Data Centre, 12, Union Road, Cambridge CB2 1EZ, UK; fax: +44 1223 336033).

Solid-State NMR Spectroscopy. The wide line ^{2}H NMR was performed on a Bruker Avance III 300 spectrometer operating at 46.07 MHz for ^{2}H. A Bruker two-channel static PE probe with a homemade 2.5 mm coil was used to record the ^{2}H spectra. The ^{2}H spectra were acquired using the solid echo sequence ($90^o - \tau - 90^o - \tau -$ acquire). The ^{2}H pulse width is 2 μs at a RF field strength of $\gamma B_1/2\pi$ = 125 kHz. Below 190 K, the used refocusing delay τ was 16 μs. Above 190 K, the refocusing delay τ of 30 μs was used. The ^{2}H patterns were simulated via the weblab (http://weblab.mpip-mainz.mpg.de/weblab/).

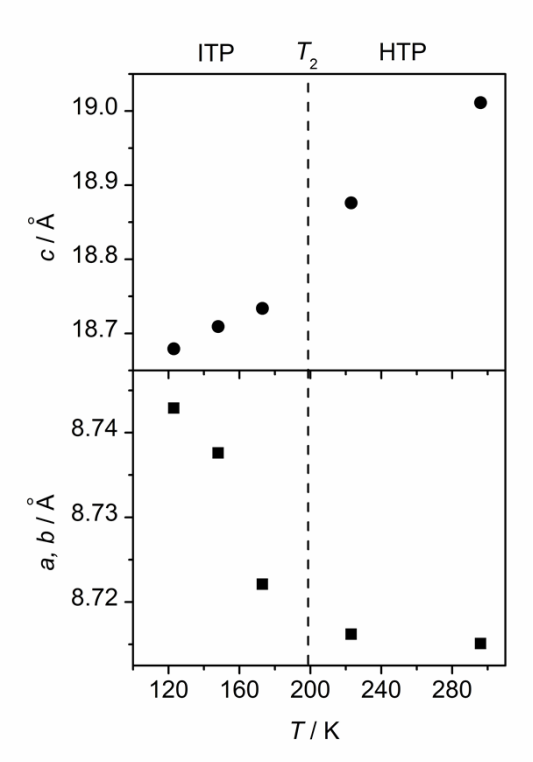

Figure S1. Temperature dependence of cell parameters of **1-d$_0$**.

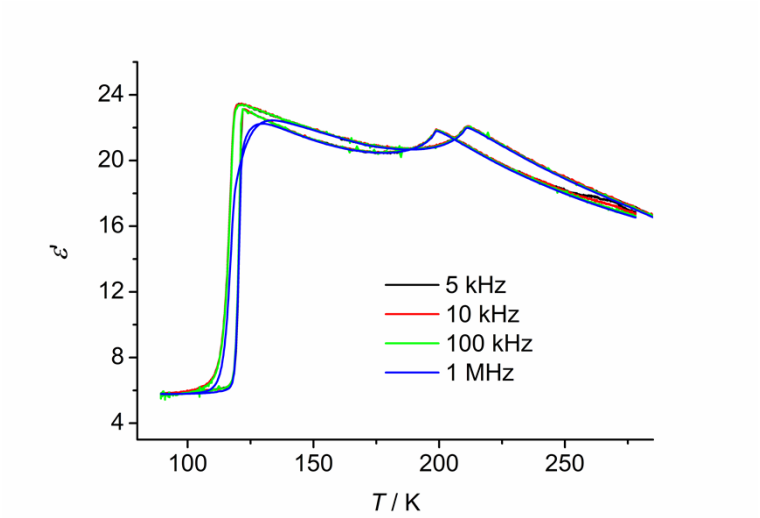

Figure S2. Temperature-dependent dielectric constants (ε′) of **1-d$_0$** along the [101] direction measured at different frequencies

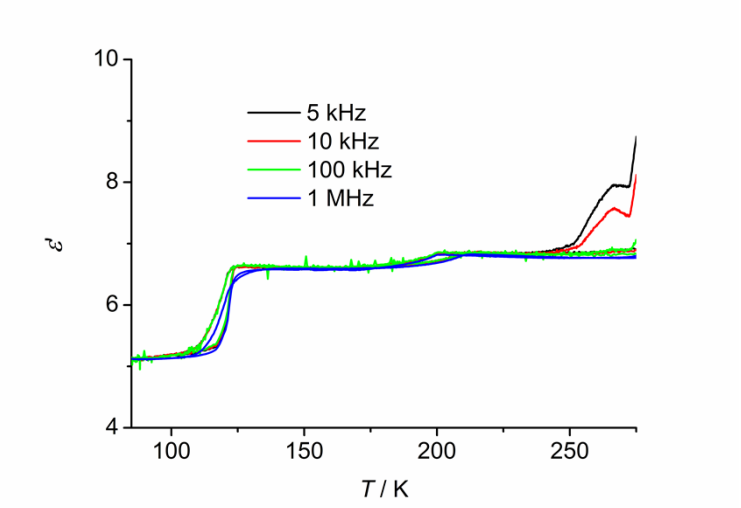

Figure S3. Temperature-dependent dielectric constants (ε′) of **1-d$_0$** along the [001] direction measured at different frequencies.

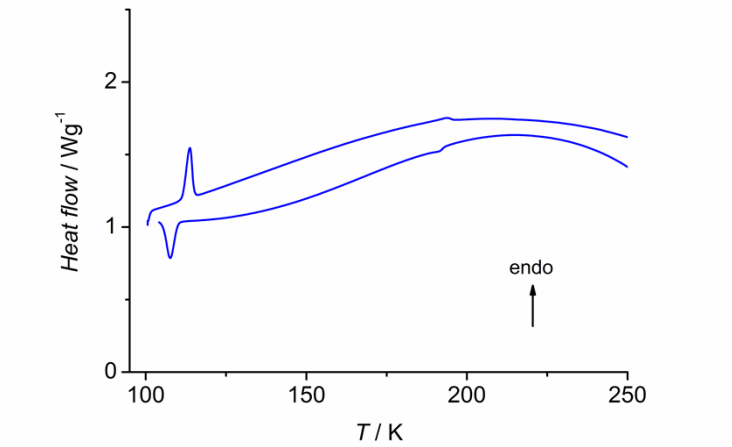

Figure S4. DSC curves of **1-d$_3$**.

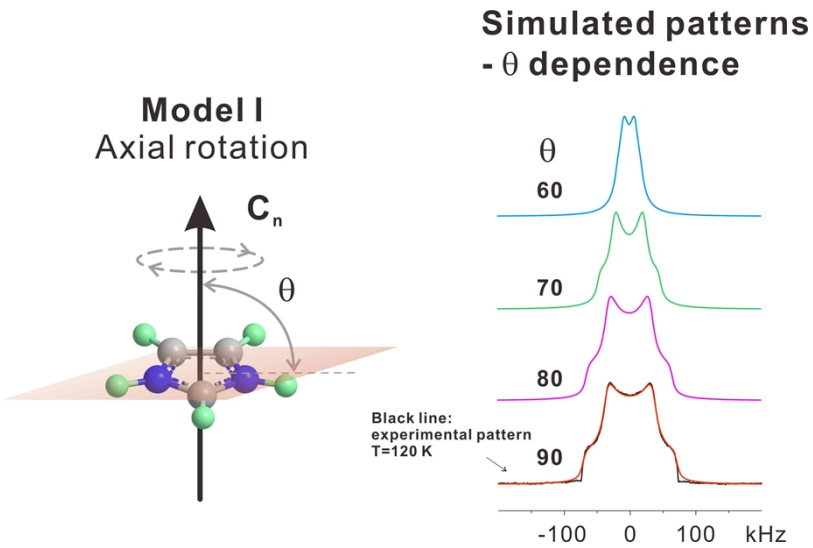

Figure S5. Axial motion of imidazolium cation (Model I). The simulated ^{2}H patterns show the influence of the angle, θ, between the rotational axis (C_n) and the molecular plane of imidazolium cation on the ^{2}H NMR lineshape. The quadrupole coupling used in the simulation is 144 kHz and the asymmetric parameter $\eta = 0$. The rotational frequency used in the simulation is 3 MHz.

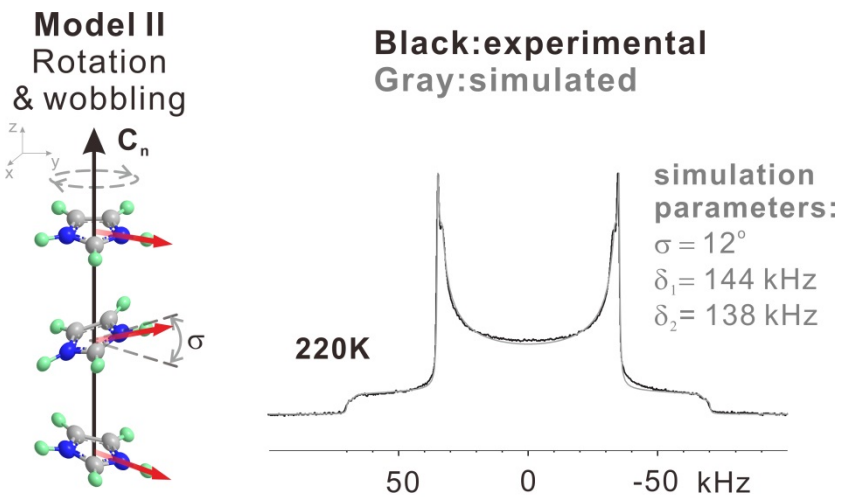

Figure S6. Motion mode of imidazolium cation in ITP (Model II). In this model, the imidazolium ring perform an axial rotation combined an out-plane oscillatory fluctuation. In the simulation, the axail rotation of imidazolium cation is assumed to be in the fast limit and the fluctuation angle is assumed to have a Gaussian distribution with a width of σ. Because N-C**D**-N and N-C**D**-C**D**-N of deuterated

imidazolium (**1-d$_3$**) are likely to have different quandrupole couplings, the right simulated pattern (gray) was obtained by summating two patterns that were simulated by using the quadrupole couplings of 138 kHz and 144 kHz, respectively, and σ = 12° in both cases. In the summation, the ratio of the two sub-patterns is 1:2. The lineshape of the simulated pattern (gray) closely resembles to the experimental pattern (black) acquired at 220 K.

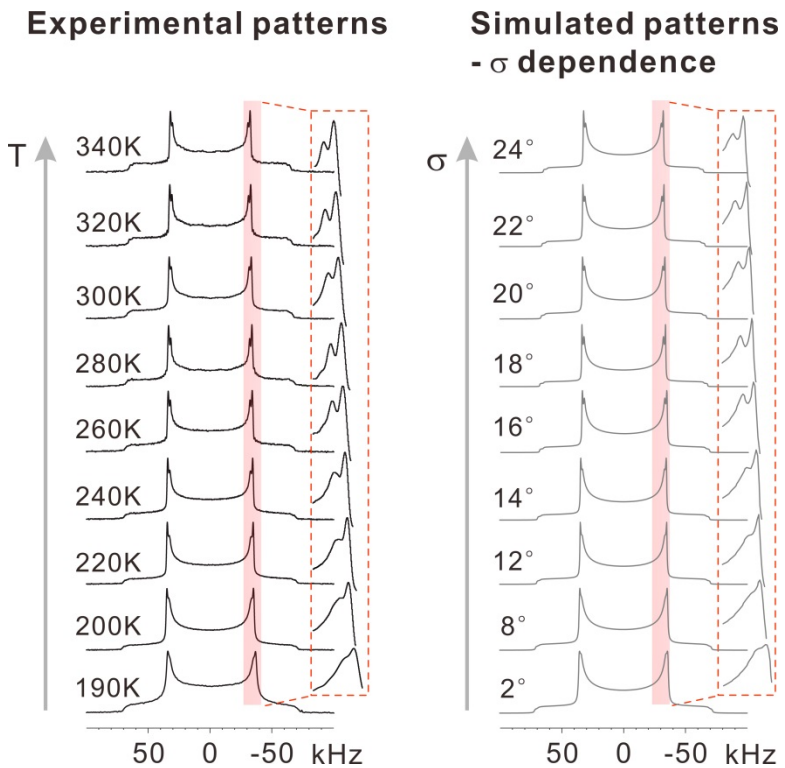

Figure S7. Left: the experimental ^{2}H patterns at the temperature range between 190 K and 340 K. **Right**: the simulated ^{2}H patterns based on Model II (i.e., the axial C_n rotation + the out-plane oscillatory fluctuation). Each simulated pattern consists of two sub-patterns simulated by using the quadrupole couplings of 138 kHz and 144 kHz, respectively, and by assuming a fluctation angle having a Gaussian distribution with a width of σ. In the simulation, the axail C_n rotation is assumed to be in the fast limit. In the summation, the ratio of the two sub-patterns is 1:2.

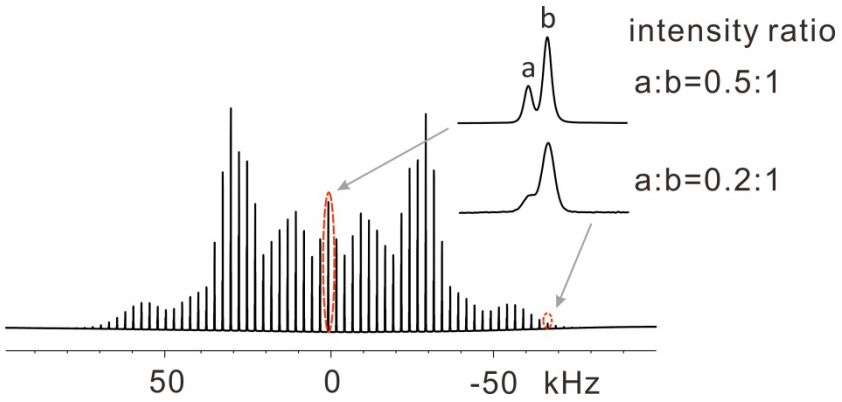

Figure S8. Solid state ^{2}H magic angle spinning spectrum of **1-d$_3$**. The spectrum was measured using the single pulse excitation pulse sequence. In the experiment, the rotation speed is 2.5 kHz and the recycle delay is 5 s. The experimental temperature is 280K.

In Figure S8, the spike-like signals are the spinning sidebands. It is observed that each spinning sideband consists of two signals. We have extracted two spinning sidebands, i.e., one from the center of the spectrum, and one from the edge of the spectrum. Decomposition shows an intensity ratio of 1:2 for the central sideband, and 1:5 for the edge sideband. We thus assigned the signals in the spinning sideband: The low field singal, a, is from N-C**D**-N, and the high field signal, b, is from N-C**D**-C**D**-N. The different intensity ratios between a and b in the different spinning sidebands are indicative of the different quandrupole couplings of N-C**D**-N and N-C**D**-C**D**-N.

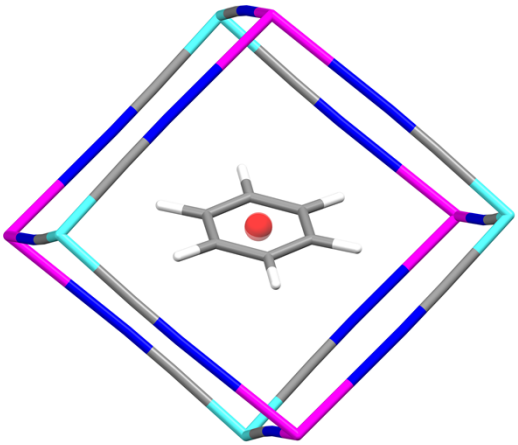

Figure S9. The centres of the equivalent negative charge and the positive charge of the HIm ring of the cage in HTP are shown as red balls with a distance of 0.036 Å.